Int. J. Solids Structures Vol. 20, No. 5, pp. 467–486, 1984
Printed in Great Britain.

0020–7683/84 \$3.00 + .00

ON THE CREEP-HARDENING RULE FOR METALS WITH A MEMORY OF MAXIMAL PRESTRESS

Z. MRÓZ and W. A. TRĄMPCZYŃSKI
Institute of Fundamental Technological Research, Warsaw, Poland

(*Received* 1 *June* 1982; *in revised form* 26 *June* 1983)

Abstract—The creep-hardening constitutive model based on the concept of kinematic hardening is discussed. The distinction is made between active and unloading creep processes and the hardening is assumed to depend on two scalar parameters α_m and α_u, the first representing the maximal prestress measure, the other corresponding to accumulated measure of unloading events. The constitutive model is applied to simulate monotonic and cyclic creep deformation in pure copper tubes subjected to combined tension and torsion at 300°C. The interaction between monotonic and cyclic hardening and the effect of initial prestress are studied and model predictions are compared with experimental data.

1. INTRODUCTION

In most phenomenological creep theories for metals[2–9], the usual assumption is made that the creep rate depends on the stress tensor and on a set of hardening parameters. By following the plasticity concepts and the isotropic or kinematic hardening rules, it is assumed that the state of isotropic hardening is represented by a monotonically growing scalar parameter λ proportional to the accumulated plastic or viscous strain and the state of anisotropic hardening is represented by a tensor parameter α interpreted as a "back stress". The evolution rule for α may describe both hardening and recovery processes within the material. The application of several creep-hardening constitutive relations to simulate creep of 304 stainless steel under monotonic and repeated loading was recently presented in [19].

The creep-hardening rule discussed in this paper is based on similar assumptions but differs from previous formulations in taking account of the memory of maximal prestress from the past loading history. The measure of maximal prestress is expressed as a supremum of the scalar norm of the back stress α. The loading processes can therefore be classified into two groups, namely, those for which the maximal prestress increases and those for which maximal prestress was reached earlier. The hardening rules are also different for those two kinds of processes. A similar concept was recently discussed in [1] for the case of plastic hardening with neglect of viscous effects and applied to simulate cyclic hardening and softening effects of several steels. The present paper extends this formulation for the case of creep at elevated temperatures. The complex phenomena occurring for creep under constant or varying stresses can thus be simulated by applying the proposed model. The important problem of creep-plasticity interaction and the associated hardening effects can also be treated within the present formulation, see [20].

A different formulation of viscoplastic constitutive relations applicable both for monotonic and variable loading was presented in [9, 10]. In [10], the scalar norm of maximal total strain was used as a measure of maximal prestrain. A general concept of rate and history dependence in metals was presented in [12] where the importance of maximal prestress on the subsequent inelastic behaviour was indicated. A two-surface model of kinematic and isotropic hardening was presented in [13], where besides the yield surface, an additional hardening surface in the strain space was introduced. This idea was next extended and modified in order to simulate creep effects in a stainless steel for variable loading[14]. Finally, the composite or multisurface creep-hardening rules[16–18] provide a natural measure of maximal prestress and allow for distinction between particular loading events through loading–unloading conditions for particular surfaces. The present formulation can be regarded as a modified version of such rules and the measure of maximal prestress is here expressed in terms of the "back stress" rather than stress itself.

In Section 2, the main model assumptions and its formulation will be presented whereas in Section 3 the model will be applied to describe biaxial creep of copper under constant tension and cyclically varying torsion stress.

2. FORMULATION OF HARDENING RULE

Consider the creep potential in the form

$$W = \frac{\mu}{n+1}(f - \sigma_p)^{n+1} \tag{1}$$

and the creep rule

$$\begin{aligned} \dot{\epsilon}^c &= \frac{\partial W}{\partial \boldsymbol{\sigma}} = \mu (f - \sigma_p)^n \frac{\partial f}{\partial \boldsymbol{\sigma}} \quad && \text{for } f - \sigma_p > 0 \\ \dot{\epsilon}^c &= 0 && \text{for } f - \sigma_p \leqslant 0 \end{aligned} \tag{2}$$

where μ and n are the material parameters and f is a homogeneous function of order one of the "effective" stress $\bar{\mathbf{s}} = \mathbf{s} - \boldsymbol{\alpha}$. Here $\mathbf{s}$ denotes the stress deviator, $\boldsymbol{\alpha}$ is the residual "back stress" tensor and σ_p denotes the yield limit. The usual small strain theory is used throughout the paper. The creep rule (2) implies that there exists an elastic domain $f - \sigma_p < 0$ within which only elastic strain increments occur and a viscous domain $f - \sigma_p > 0$ lying in the exterior of the elastic domain. As we are interested in this paper in high-temperature creep, it will be set $\sigma_p = 0$, thus assuming that the elastic domain shrinks to a point. However, a more accurate model, applicable to moderate or room temperature creep would require the assumption of existence of the elastic domain. In particular, when studying plastic hardening at room temperature, the evolution rule for σ_p becomes the most important component of the constitutive model, as it was demonstrated in [1].

Assume f to be a function of the form

$$f = \bar{\sigma}_e = \left[\frac{3}{2}(\mathbf{s} - \boldsymbol{\alpha}) \cdot (\mathbf{s} - \boldsymbol{\alpha})\right]^{1/2} \tag{3}$$

where the dot between two symbols denotes their scalar product (or trace operation for two tensors). To introduce the measure of maximal prestress, let us introduce, similarly as in [1] the scalar norm of $\boldsymbol{\alpha}$ in the form

$$\alpha_e = \left(\frac{3}{2}\boldsymbol{\alpha} \cdot \boldsymbol{\alpha}\right)^{1/2} \tag{4}$$

and the maximal value of α_e reached during the creep process will be denoted by α_m, that is

$$\alpha_m = \sup_{0<s<t} \alpha_e \, (t - s). \tag{5}$$

During the initial creep process α_e increases from its initial value and then $\alpha_e = \alpha_m$, $\dot{\alpha}_e = \dot{\alpha}_m$. On the other hand, when after reaching the maximal value $\alpha_e = \alpha_m$, its subsequent value decreases, $\alpha_e < \alpha_m$, then the maximal value α_m is kept in the material memory and a new creep process commences.

The distinction can therefore be made between two types of creep processes: *the active creep process* for which $\dot{\alpha}_e = \dot{\alpha}_m$, $\alpha_e = \alpha_m$, and *the creep unloading process* for which $\alpha_e < \alpha_m$. In the following, we shall discuss consecutively the constitutive relations for these two creep processes.

For the active creep process, the creep rule (2), in view of (3) takes the form

$$\dot{\epsilon}^c = \mu(f-\sigma_p)^n \frac{3(\mathbf{s}-\boldsymbol{\alpha})}{2f} \tag{6}$$

and for $\sigma_p = 0$, there is

$$\dot{\epsilon}^c = \mu f^{n-1} \frac{3}{2}(\mathbf{s}-\boldsymbol{\alpha}). \tag{7}$$

In formulating the evolution rule for $\boldsymbol{\alpha}$, it can be assumed, similarly as in [8] that this rule should represent plastic (or creep) hardening and both plastic and viscous recovery processes, that is

$$\dot{\boldsymbol{\alpha}}^{(f)} = C_1^{(f)}\dot{\epsilon}^c - C_2^{(f)}\boldsymbol{\alpha}\dot{\lambda} - C_3^{(f)}\boldsymbol{\alpha} \tag{8}$$

where

$$\dot{\lambda} = \left(\frac{2}{3}\dot{\epsilon}^c \cdot \dot{\epsilon}^c\right)^{1/2}, \quad \lambda = \int_0^t \dot{\lambda}\,dt \tag{9}$$

and $C_1^{(f)}$, $C_2^{(f)}$ and $C_3^{(f)}$ are material functions of α_e and σ_e to be specified. The first term of (8) represents a familiar kinematic hardening whereas the two remaining terms correspond to plastic and viscous recovery. An alternative evolution rule for $\boldsymbol{\alpha}$ was discussed in [2] where the back stress was assumed to be composed of two portions $\boldsymbol{\alpha}_1$ and $\boldsymbol{\alpha}_2$ undergoing recovery specified by two different rules.

In considering the evolution rules for copper, the explicit expression for viscous recovery term in (8) will be neglected for active creep processes and the rule (8) will be replaced by a simpler form

$$\dot{\boldsymbol{\alpha}}^{(f)} = C_1^{(f)}\boldsymbol{\beta}^{(f)}\dot{\lambda} \quad \text{for } \alpha_e = \alpha_m,\ \dot{\alpha}_e > 0 \tag{10}$$

where

$$\boldsymbol{\beta}^{(f)} = \frac{\boldsymbol{\sigma}-\boldsymbol{\alpha}}{[(\boldsymbol{\sigma}-\boldsymbol{\alpha})\cdot(\boldsymbol{\sigma}-\boldsymbol{\alpha})]^{1/2}} \tag{11}$$

is the unit vector specifying the direction of evolution of $\boldsymbol{\alpha}$. The recovery effect will be incorporated into the function $C_1^{(f)} = C_1^{(f)}(\alpha_e, \sigma_e)$, so that the steady creep process will be attained for any stress level.

The active creep process can be represented both in the stress or back stress spaces, Fig. 1. To indicate the analogy with a multisurface hardening rule proposed in [18], consider first the representation in the stress space, Fig. 1(a). Consider the yield surface $f_0 = 0$ which is initially centered at the origin 0. When the stress state represented by the point P_1 is applied and next kept fixed, the creep process governed by (2) or (6) commences and the evolution of $\boldsymbol{\alpha}$ governed by (10) occurs. The yield surface translates toward the stress point P_1. Introduce, besides the yield surface, a set of nesting surfaces $f_1 = 0$, $f_2 = 0, \ldots F = 0$ of the same shape and growing sizes, analogous to those discussed in [18] for the case of plastic hardening. The consecutive surfaces engage each other without intersection and for the active creep process the surface $f_l = 0$ undergoes translation once it becomes engaged by the surface $f_{l-1} = 0$. In Fig. 1(a) the nesting surfaces and the yield surface are tangential at R_1 and the outermost surface $F = 0$ is centered at 0. This surface provides a measure of maximal prestress for changing stress state. Consider, for instance, the case when the stress point is changed to P_2 and kept fixed at P_2 for some time. During the creep unloading process the yield surface will translate inside the domain $F \leqslant 0$, and eventually becomes tangential to the maximal prestress surface $F = 0$. Consider the point R_2 on $f_0 = 0$ associated with the stress point P_2, so that both P_2 and R_2 lie on the line A_1P_2 connecting the center of $f_0 = 0$ with P_2. It can be postulated that the instantaneous motion

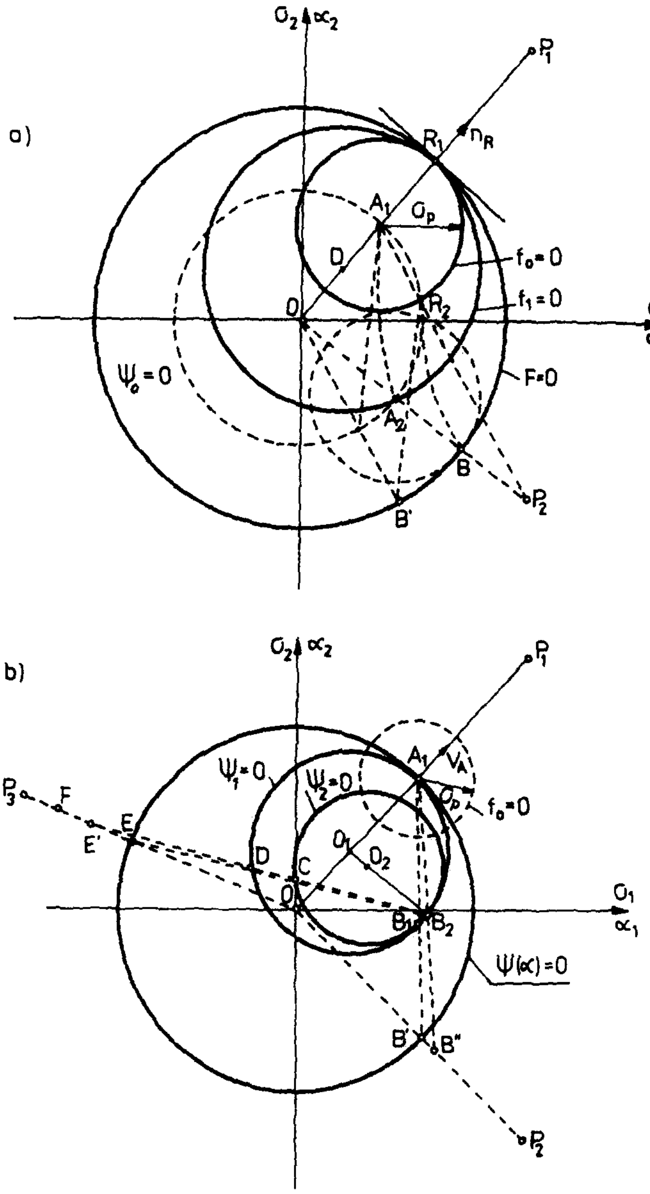

Fig. 1. The evolution of the back stress α for stress state at P_1 with subsequent change to P_2 and P_3; (a) evolution following from the multisurface hardening model, (b) evolution in the α-space.

of R_2 is directed to the respective point on the consecutive surface having the same normal direction, that is along R_2B', where $0B'$ is parallel to A_1R_2. The subsequent creep process will involve motion of the yield and nesting surfaces lying inside the surface $F = 0$ and they eventually become tangential to $F = 0$ at the point B lying on the radial line $0P_2$. The center of the yield surface moves along the path A_1A_2 and the creep unloading process terminates when the yield surface engages the maximal prestress surface at B.

Let us note that instead of the maximal prestress surface $F = 0$ in the stress space we can introduce the maximal loading surface in the α-space, namely

$$\psi_0(\alpha, 0) = \alpha_e - \alpha_m = 0 \tag{12}$$

so that for the active creep process there is

$$\alpha_e = \alpha_m, \qquad \dot{\alpha}_e = \dot{\alpha}_m > 0 \tag{13}$$

and the diameter of $\psi_0 = 0$ is monotonically growing. This representation seems convenient since the evolution rules for $\boldsymbol{\alpha}$ can now be formulated independently of the relative configuration of nesting surfaces. In the following, we shall develop our model by using the representation in the $\boldsymbol{\alpha}$-space.

Referring to Fig. 1(b), it is seen that the active creep process terminates at A_1 when the stress state is changed from P_1 to P_2 and subsequently kept fixed at P_2. Assume that the elastic domain $f_0 \leqslant 0$ is shrinked to a point, thus $\sigma_p = 0$. The creep unloading process starts when the $\boldsymbol{\alpha}$-path moves into the interior of the domain enclosed by the maximal loading surface $\psi_0 = 0$, that is α_e starts to decrease from its maximal value α_m reached at the point A. To specify the measure of creep unloading, let us introduce another surface within this domain, similar to the surface $\psi_0 = 0$ and tangential to it at A, thus

$$\psi_1(\boldsymbol{\alpha}, \boldsymbol{\alpha}_0^{(1)}) = \left[\frac{3}{2}(\boldsymbol{\alpha} - \boldsymbol{\alpha}_0^{(1)}) \cdot (\boldsymbol{\alpha} - \boldsymbol{\alpha}_0^{(1)})\right]^{1/2} - \alpha_u^{(1)} = 0 \tag{14}$$

where $\boldsymbol{\alpha}_0^{(1)}$ denotes the center position of the surface (14) and $\alpha_u^{(1)}$ is proportional to its radius. For the creep unloading path A_1B_2, the surface $\psi_1 = 0$ passes through A_1 and B_2, hence

$$\frac{3}{2}(\boldsymbol{\alpha}_A - \boldsymbol{\alpha}_0^{(1)}) \cdot (\boldsymbol{\alpha}_A - \boldsymbol{\alpha}_0^{(1)}) - (\alpha_u^{(1)})^2 = 0$$

$$\frac{3}{2}(\boldsymbol{\alpha}_B - \boldsymbol{\alpha}_0^{(1)}) \cdot (\boldsymbol{\alpha}_B - \boldsymbol{\alpha}_0^{(1)}) - (\alpha_u^{(1)})^2 = 0 \tag{15}$$

and from (15) it follows that

$$\alpha_u^{(1)} = \sqrt{\frac{3}{2}}\frac{(\boldsymbol{\alpha}_B - \boldsymbol{\alpha}_A) \cdot (\boldsymbol{\alpha}_B - \boldsymbol{\alpha}_A)}{2(\boldsymbol{\alpha}_B - \boldsymbol{\alpha}_A) \cdot \mathbf{v}_A} = \sqrt{\frac{3}{2}}r^{(1)} \tag{16}$$

$$\boldsymbol{\alpha}_0^{(1)} = \boldsymbol{\alpha}_A - \mathbf{v}_A r^{(1)} \tag{17}$$

where $\boldsymbol{\alpha}_B$ and $\boldsymbol{\alpha}_A$ denote the positions of the instantaneous back stress at the point B_2 and at the contact point A_1, whereas $\mathbf{v}_A$ denotes the unit vector along 0_1A_1, Fig. 1(b). The radius of the surface $\psi_1 = 0$ is denoted by $r^{(1)}$. Let us note that the surface $\psi_1 = 0$ is similar to the maximal loading surface $\psi_0 = 0$ and coincides with it when $\boldsymbol{\alpha}_0^{(1)} = 0$ and $\alpha_u^{(1)} = \alpha_m^{(1)}$. The relations (17) and (18) can be regarded as evolution equations for $\alpha_u^{(1)}$ and $\boldsymbol{\alpha}_0^{(1)}$ expressed in terms of $\boldsymbol{\alpha}_A$ and $\boldsymbol{\alpha}_B$. Though they are not rate equations, the complete description is provided when the evolution rule of $\boldsymbol{\alpha}_B$ is formulated as the rate equation.

The *first creep unloading event* is defined by the inequalities

$$\dot{\alpha}_u^{(1)} > 0, \qquad \alpha_u^{(1)} < \alpha_m^{(1)}. \tag{18}$$

The *second creep unloading event* commences when at some point B there is $\alpha_u^{(1)} < 0$ and the $\boldsymbol{\alpha}$-path penetrates into the domain enclosed by the surface $\psi_1 = 0$. Similarly, as previously, let us construct a new surface

$$\psi_2(\boldsymbol{\alpha}, \boldsymbol{\alpha}_0^{(2)}) = \left[\frac{3}{2}(\boldsymbol{\alpha} - \boldsymbol{\alpha}_0^{(2)}) \cdot (\boldsymbol{\alpha} - \boldsymbol{\alpha}_0^{(2)})\right]^{1/2} - \alpha_u^{(2)} = 0 \tag{19}$$

passing through B_1 and C and being tangential at B_2 to $\psi_1 = 0$, Fig. 1(b). The second creep unloading event continues when

$$\dot{\alpha}_u^{(2)} > 0, \qquad \alpha_u^{(2)} < \alpha_u^{(1)} \tag{20}$$

and for $\alpha_u^{(2)} = \alpha_u^{(1)}$ the surface $\psi_2 = 0$ merges with the surface $\psi_1 = 0$. For the subsequent path DE in the exterior of $\psi_1 = 0$, the second creep unloading event is erased from the material memory. For the $\boldsymbol{\alpha}$-path EF in the exterior of $\psi_0 = 0$, the active creep process continues and the relations (7) and (10) apply.

The relations (16)–(20) should be complemented by the evolution rule for $\boldsymbol{\alpha}$ during the creep unloading process. This rule will provide, in particular, the instantaneous value $\boldsymbol{\alpha}_B$ in (16) and (17), when $\alpha_u^{(1)}$ and $\alpha_0^{(1)}$ are specified. Whereas the creep rule (6) or (7) remains valid, the evolution rule for $\boldsymbol{\alpha}$ is modified for the creep unloading process, namely

$$\dot{\boldsymbol{\alpha}}^{(u)} = C_1^{(u)}(\alpha_m, \alpha_u)\boldsymbol{\beta}^{(u)} + \dot{\boldsymbol{\alpha}}^{(l)}, \quad \text{for } \alpha_e < \alpha_m,\ \dot{\alpha}_u > 0 \tag{21}$$

where $\boldsymbol{\beta}^{(u)}$ is the unit vector. The first term of (21) represents the unloading recovery term that vanishes when $\alpha_u = \alpha_m$, whereas the second term represents the continuing hardening. It can be speculated that the instantaneous direction of $\boldsymbol{\beta}^{(u)}$ coincides with the vector $\mathbf{s} - \boldsymbol{\alpha}$ for all values of stress. However, following the discussion of evolution rule in the stress space for multisurface model, Fig. 1(a), it is assumed that the vector $\boldsymbol{\beta}^{(u)}$ coincides with $\mathbf{s} - \boldsymbol{\alpha}$ only for stress states lying inside the surface $\psi_0 = 0$ whereas for stress states in the exterior of this surface, the $\boldsymbol{\alpha}$-path of the unloading recovery is directed to a point B' lying on $\psi_0 = 0$ and the radial line $0P_2$ connecting the center of ψ_0 with the stress point. It can therefore be assumed in the evolution rule (21) that

$$\begin{aligned} \boldsymbol{\beta}^{(u)} &= \frac{\mathbf{s} - \boldsymbol{\alpha}}{[(\mathbf{s} - \boldsymbol{\alpha}) \cdot (\mathbf{s} - \boldsymbol{\alpha})]^{1/2}} \quad \text{for } \sigma_e = \left(\frac{3}{2}\mathbf{s} \cdot \mathbf{s}\right)^{1/2} < \alpha_m \\ \boldsymbol{\beta}^{(u)} &= \frac{\bar{\mathbf{s}} - \boldsymbol{\alpha}}{[(\bar{\mathbf{s}} - \boldsymbol{\alpha}) \cdot (\bar{\mathbf{s}} - \boldsymbol{\alpha})]^{1/2}} \quad \text{for } \sigma_e > \alpha_m \end{aligned} \tag{22}$$

where

$$\bar{\mathbf{s}} = \mathbf{s}\frac{\alpha_m}{\sigma_e}. \tag{23}$$

This evolution rule is illustrated in Fig. 1(b). For the stress point at P_1, the $\boldsymbol{\alpha}$-path $0A_1$ follows the radial line $0P_1$ until the point A_1 is reached. When the stress state is subsequently changed and is represented by a point P_2, the creep unloading process occurs. The first term of (21) predicts the $\boldsymbol{\alpha}$-path following the line A_1B_1B' terminating at B' lying on the radial line $0P_2$ and on the surface $\psi_0 = 0$ whereas the second term of (21) predicts the evolution direction along the line connecting P_2 with the instantaneous $\boldsymbol{\alpha}$-point. As the first term predominates, the $\boldsymbol{\alpha}$-path A_1B_2B'' departs slightly from the line A_1B_1B'. The subsequent evolution of $\boldsymbol{\alpha}$ follows the line $B''P_2$. If the stress point is changed to P_3 with $\boldsymbol{\alpha}$ represented by B_2, the respective evolution of $\boldsymbol{\alpha}$ would follow the path B_2E' whereas the first term of (21) would correspond to the path B_2E, Fig. 1(b). The evolution paths of $\boldsymbol{\alpha}$ in Fig. 1(b) can be regarded as simplified version of paths following from the multisurface translation rule, Fig. 1(a). Whereas the unloading path A_1A_2 in Fig. 1(a) is curvilinear, the path A_1B_1 in Fig. 1(b) is assumed as a straight line.

The function $C_1^{(u)}$ occurring in (21) should satisfy the condition that $\dot{\alpha}^{(u)} = \dot{\alpha}^{(l)}$ for $\alpha_m = \alpha_u$. This function is therefore expressed in the form

$$C_1^{(u)} = B(\alpha_m - \alpha_u)^k \tag{24}$$

where B and k are material parameters.

To complete the formulation of our model, the evolution rule (10) should be more precisely specified. This rule should describe the material hardening during both active and unloading processes. Assume that for the active creep process α_m tends to its asymptotic value α_f being in general a function of the effective stress σ_e. Thus, for any fixed stress level, the material tends toward a steady creep process occurring at the constant rate of creep. Here α_f resembles much the concept of a friction stress discussed by Parker and Wilshire[11]. If on the other hand, the active creep process is interrupted and the creep unloading process proceeds, the value of α_f can further be modified due to additional hardening. To introduce a proper measure for hardening during the creep unloading events, let us introduce the accumulated measure of α defined as follows

$$\alpha_a = \sum_{i=1}^{k} \Delta\alpha_u^{(i)} \quad \text{for } \alpha_e < \alpha_m \tag{25}$$

where $\Delta\alpha_u^{(i)}$ is the maximal value of $\alpha_u^{(i)}$ attained during the ith creep unloading event. On the other hand, when the creep unloading process is interrupted and the active process proceeds for which α_m grows further, a new count of α_a is made for successive creep unloading events. Assume that for the active creep process, the evolution rule (10) takes the form

$$\dot{\boldsymbol{\alpha}}^{(l)} = A(\alpha_f^{(0)} - \alpha_m)\cdot \boldsymbol{\beta}^{(l)} \cdot \dot{\lambda}, \qquad \alpha_e = \alpha_m, \qquad \dot{\alpha}_m > 0 \tag{26}$$

where A is the material parameter. For the subsequent creep unloading process ($\alpha_e < \alpha_m$), the value $\alpha_f^{(0)}$ is assumed to be modified by the following rule

$$\alpha_f^{(1)} = \alpha_f^{(0)} \cdot G(\alpha_a) = \alpha_f^{(0)} \frac{1+\beta\alpha_a}{1+\gamma\alpha_a} \tag{27}$$

where β and α are the material parameters and $G(\alpha_a) = 1$ for $\alpha_a = 0$, $G(\alpha_a) = (\beta/\gamma)$ for $\alpha_a \to \infty$. Thus for $\alpha_a \to \infty$, there is $\alpha_f^{(1)} = \alpha_f^{(0)}(\beta/\gamma)$ and if $(\beta/\gamma) > 1$, the asymptotic value of the friction stress is augmented due to hardening developed during creep unloading events. If now the creep loading process is next followed, a new value $\alpha_f^{(1)}$ determined by (27) is substituted into (26), thus

$$\dot{\boldsymbol{\alpha}}^{(l)} = A(\alpha_f^{(1)} - \alpha_m)\cdot \boldsymbol{\beta}^{(l)} \cdot \dot{\lambda}, \quad \dot{\alpha}_m > 0 \tag{28}$$

and similarly, the new value $\alpha_f^{(1)}$ is substituted into (27) to compute $\alpha_f^{(2)}$ during the successive creep unloading process. The interaction between active and unloading creep events can therefore be studied by following the rules (26)–(28). Physically, it can be speculated that the active loading process creates a dislocation structure which is afterwards slightly modified due to motion of mobile dislocations during the creep unloading events. This modification is roughly accounted for in the rule (27).

When the creep process proceeds initially under high stress which is subsequently reduced, it is possible that the value of α_f reached during the first period is higher than the value of α_f during the second period. This situation may occur when α_f is a monotonic function of the effective stress, $\alpha_f = \alpha_f(\sigma_e)$. The evolution rule (26) would then imply diminuation of α_m during the second period, that is recovery of α_m to a lower value. It can be expected that such recovery (similar to softening effect occurring during cyclic loading at room temperature) occurs actually in metals but it is not clear how significantly is may reduce the previous hardening. Neglecting this effect for copper, it is assumed that

$$\dot{\boldsymbol{\alpha}}^{(l)} = 0, \quad \dot{\alpha}_f = 0 \qquad \text{when} \qquad \alpha_m > \alpha_f. \tag{29}$$

In other words, when $\alpha_e = \alpha_m$ reaches a value that is higher than the asymptotic friction stress α_f corresponding to lower values of the effective stress during subsequent stages of active creep, the recovery of α_m is neglected.

Let us now provide a brief recapitulation of model equations. As we have seen, there are three major components of the model, namely *creep*, *hardening evolution* and *memory rules*. We shall consecutively outline governing equations for these rules.

(i) *Creep rule*. As we set $\sigma_p = 0$, that is neglect the elastic domain, the creep rule obeys eqn (7), that is

$$\dot{\boldsymbol{\epsilon}}^c = \mu f^{n-1} \frac{3}{2}(\mathbf{s} - \boldsymbol{\alpha}) \tag{30}$$

where $f = \bar{\sigma}_e$ is specified by (3) and μ is the material parameter. This creep rule is valid for both active and unloading creep processes.

(ii) *Hardening evolution rule* specifies the evolution of the back stress $\boldsymbol{\alpha}$. This evolution rule is different for active and unloading creep processes. There is $\dot{\boldsymbol{\alpha}} = \dot{\boldsymbol{\alpha}}^{(l)}$ for $\alpha_e = \alpha_m$, $\dot{\alpha}_e > 0$ and $\dot{\boldsymbol{\alpha}} = \dot{\boldsymbol{\alpha}}^{(u)}$ for $\alpha_e < \alpha_m$ or $\alpha_e = \alpha_m$, $\dot{\alpha}_e < 0$. For the active creep process, according to (26) and (27) there is

$$\dot{\boldsymbol{\alpha}}^{(l)} = A(\alpha_f - \alpha_m) \cdot \boldsymbol{\beta}^{(l)} \cdot \dot{\lambda}, \quad \alpha_f > \alpha_m$$
$$\dot{\boldsymbol{\alpha}}^{(l)} = 0 \qquad\qquad \alpha_f < \alpha_m \tag{31}$$

where

$$\dot{\alpha}_f = \alpha_f^{(0)}(\sigma_e) \cdot G(\alpha_a) \tag{32}$$

is the friction stress corresponding to the maximal value of α_m reached in the creep process under constant stress. The function $G(\alpha_a)$ specified by (27) accounts for additional hardening during creep unloading processes. In fact for the first active creep process there is $G(\alpha_a) = 1$ and α_f is specified by the applied stress level. On the other hand, for unloading creep processes, there is an additional growth of α_f due to variation of $G(\alpha_a)$. For consecutive active and unloading creep processes the relation (32) applies with α_a measured from zero for each new unloading event. Thus, for the second unloading event, there is

$$\alpha_f^{(2)} = \alpha_f^{(0)}(\sigma_e) \cdot G(\alpha_{a_1}) \cdot G(\alpha_{a_2}) \tag{33}$$

where α_{a_1} and α_{a_2} are the values of α_a reached during the first and the second unloading event. The value $\alpha_f^{(2)}$ is next used in (31) in the evolution rule for active creep loading.

For creep unloading events, the evolution rule (21) applies with $\boldsymbol{\beta}^{(u)}$ specified by (23) and $C_1^{(u)}$ specified by (24), thus

$$\dot{\boldsymbol{\alpha}}^{(u)} = B(\alpha_m - \alpha_u)^k \cdot \boldsymbol{\beta}^{(u)} + \dot{\boldsymbol{\alpha}}^{(l)} \tag{34}$$

and $\dot{\boldsymbol{\alpha}}^{(u)} = \dot{\boldsymbol{\alpha}}^{(l)}$ when $\alpha_m = \alpha_u$.

(iii) *Memory rule.* This rule is specified by introducing the maximal loading and unloading surfaces (12) and (14), (19). For the active creep process, only the instantaneous value of α_m and the value of α_f specified by (32) are remembered whereas for the unloading creep event, the value of α_m specifying the maximal prestress and the values $\alpha_u^{(l)}$, $\boldsymbol{\alpha}_0^{(i)}$ specifying the actual unloading event are remembered. Moreover, the past unloading events of greater magnitude than the recent event are stored in the memory, that is the pairs $\alpha_u^{(k)}$, $\boldsymbol{\alpha}_0^{(k)}$ for which $\alpha_u^{(k)} > \alpha_u^{(i)}$.

3. DESCRIPTION OF CYCLIC CREEP OF COPPER UNDER COMBINED TENSION AND TORSION

Let us now apply the derived constitutive relations to the case of plane stress with two non-vanishing stress components σ_x and τ_{xy} referred to a Cartesian x, y-system. Such stress state occurs in a thin walled tube subjected to tension and torsion and model predictions will be compared with test results.

The creep potential is now expressed as follows

$$W = \frac{\mu}{n+1} \bar{\sigma}_e^{n+1} \tag{35}$$

where

$$\bar{\sigma}_e = [(\sigma_x - \alpha_x)^2 + 3(\tau_{xy} - \alpha_{xy})^2]^{1/2} \tag{36}$$

and the creep rule (7) takes the form

$$\dot{\epsilon}_x^c = \mu \cdot \bar{\sigma}_e^{n-1} \cdot 2(\sigma_x - \alpha_x), \quad \dot{\gamma}_{xy} = \mu \cdot \bar{\sigma}_e^{n-1} \cdot \sigma \cdot (\tau_{xy} - \alpha_{xy}). \tag{37}$$

Alternatively this creep rule can be expressed in a form applied usually in literature, namely

$$\frac{\dot{\epsilon}_x{}^c}{\dot{\epsilon}_0}=\left(\frac{\bar{\sigma}_e}{\sigma_0}\right)^{n-1}\frac{\sigma_x-\alpha_x}{\sigma_0},\quad \frac{\dot{\gamma}_{xy}{}^c}{\dot{\epsilon}_0}=\left(\frac{\bar{\sigma}_e}{\sigma_0}\right)^{n-1}\frac{3(\tau_{xy}-\alpha_{xy})}{\sigma_0} \tag{38}$$

where σ_0 and $\dot{\epsilon}_0$ are the material parameters. The maximal prestress is now expressed in terms of the norm

$$\alpha_e=(\alpha_x{}^2+3\alpha_{xy}{}^2)^{1/2}. \tag{39}$$

Consider first the creep for the uniaxial stress state, for instance, in tension and compression. For the active creep process, the evolution rule (28) can be expressed as follows

$$\dot{\alpha}_x{}^{(l)}=A(\alpha_f{}^{(0)}-\alpha_x{}^{(l)})\cdot\dot{\epsilon}_x{}^c \tag{40}$$

which after integration for constant $\alpha_f{}^{(0)}$ provides the finite relation

$$\alpha_x{}^{(l)}=\alpha_f{}^{(0)}[1-\exp(-A\epsilon_x{}^c)]. \tag{41}$$

It is seen that for $\epsilon_x{}^c\to\infty$ there is $\alpha_x\to\alpha_f{}^{(0)}$ and $C_1{}^{(l)}\to 0$ whereas for $\epsilon_x{}^c=0$ there is $C_1{}^{(l)}=A\alpha_f{}^{(0)}$ and $\alpha_x{}^{(l)}=0$. Similarly, for the creep unloading process, according to (34) there is

$$\dot{\alpha}_x{}^{(u)}=-\sqrt{\frac{2}{3}}B(\alpha_m-\alpha_u)^k+\dot{\alpha}_x{}^{(l)}. \tag{42}$$

3.1 *Experimental results and their analysis*

Creep tests were conducted for commercially pure copper† at constant temperature 300°C. Thin-walled tubular specimens (outer diameter 25.4 mm, thickness h = 1.7 mm and gauge length L = 38 mm) were subjected to tension–torsion in a special purpose testing machine. Details of the testing apparatus, in which the tension and torsion loading systems were decoupled using an air bearing, and of strain measurements are described in [15]. The material parameters occurring in the creep law (38) were identified, using standard procedure based on Norton's law

$$\frac{\dot{\epsilon}}{\dot{\epsilon}_0}=\left(\frac{\sigma}{\sigma_{0N}}\right)^n \tag{43}$$

applied to constant-stress creep tests under biaxial stress state (tension–torsion). The experimental effective stress-effective strain rate data are shown in Fig. 2 and the creep parameters mentioned above were found, to be:

$$n=7.2,\quad \sigma_{0N}=28.43[\mathrm{MPa}],\quad \dot{\epsilon}_0=4.2\times 10^{-3}[\%/h].$$

The experimental data shows the scatter of max. 5% in stress level, which is less than typical scatter usually occurring in creep data and may be due to material variations, specimen bending and inaccuracy in temperature control. Because of this effect, the stress correction in theoretical solutions was taken into account. To reconcile creep law (43) with the expression from (38) namely:

$$\frac{\dot{\epsilon}_x}{\dot{\epsilon}_0}=\left(\frac{\sigma_x-\alpha_f}{\sigma_0}\right)^n, \tag{44}$$

it is assumed that $\alpha_f=\eta\cdot\sigma_e$, where η is a constant parameter and $\dot{\epsilon}_0$ has the same value

†Tough pitch high conductivity copper of 99.9% purity manufactured to British Standard Specification B.S.2873 CIDI.

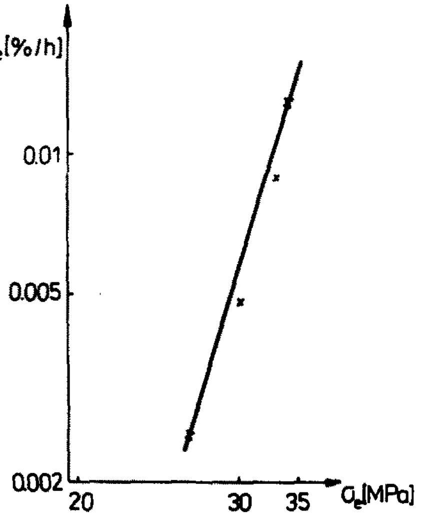

Fig. 2. The experimental dependence of creep rate on the stress level for copper.

in (43) and (44). Requiring (43) and (44) to predict the same creep rate, it is obtained that $\sigma_0 = \sigma_{0N}(1 - \eta)$. In other words, the value of σ_0 is obtained from the respective value of σ_{0N} of Norton's law.

As it was mentioned before, α_f can be interpreted as the friction stress ($\alpha_f = \eta \cdot \sigma$) extensively studied in [19]. It was found that for polycrystalline copper at 413°C under uniaxial tension $\sigma_x = 30 \div 70$[MPa] the value of η equals $0.37 \div 0.26$ and for the stress level similar to that applied in our experimental programme there is $\eta \approx 0.35$. So, in spite of difference in testing temperature, $\alpha_f^{(0)} = 0.35 \cdot \sigma_e$ was assumed in the present work. Experimental results, as it will be shown later, confirm validity of this assumption.

The uniaxial stress–strain curve for specimens tested at 300°C at a constant strain rate $\dot{\epsilon}_x = 10^{-4}\,\mathrm{s}^{-1}$ is shown in Fig. 3.

In order to verify the present model, three experimental creep programmes were carried out. Let us describe them consecutively.

(i) *Programme* 1. *Monotonic and cyclic creep hardening*

This programme consisting of eight steps, is shown in Fig. 4. In step 1, the material was instantaneously subjected to combined stress $\sigma_x = 22.723$[MPa], $\tau_{xy} = 7.712$[MPa] until the steady creep state was reached. Subsequently, during four consecutive steps, the shear stress was cyclically varied between the values ± 7.712[MPa] until the steady creep was reached at each step. During the step 6, the higher stress $\sigma_x = 26.3$[MPa] was applied and during subsequent steps 7 and 8 the shear stress was respectively $\tau_{xy} = -8.76$[MPa] and $\tau_{xy} = 8.76$[MPa]. Steady creep was attained at the end of each step. The presented programme can therefore be divided into four stages:

—stage 1: initial loading, step 1, $\sigma_e = 26.355$[MPa],
—stage 2: cyclic loading in torsion, steps 2–5, $\sigma_e = 26.355$[MPa],
—stage 3: subsequent loading, step 6, $\sigma_e = 30.366$[MPa],
—stage 4: cyclic loading in torsion, steps 7, 8, $\sigma_e = 30.366$[MPa].

This loading programme is schematically shown in Fig. 4(a, b) and both the experimental and predicted response curves $\epsilon_x = \epsilon_x(t)$ and $\gamma_{xy} = \gamma_{xy}(t)$ are shown in Fig. 4. The experimental results exhibit instantaneous strain increments after each reversal of shear stress. It is believed that these increments are not only associated with the elastic strain increments of the specimen but also with property of testing apparatus. Because the proposed theory does not contain the effect of time independent strains and because testing

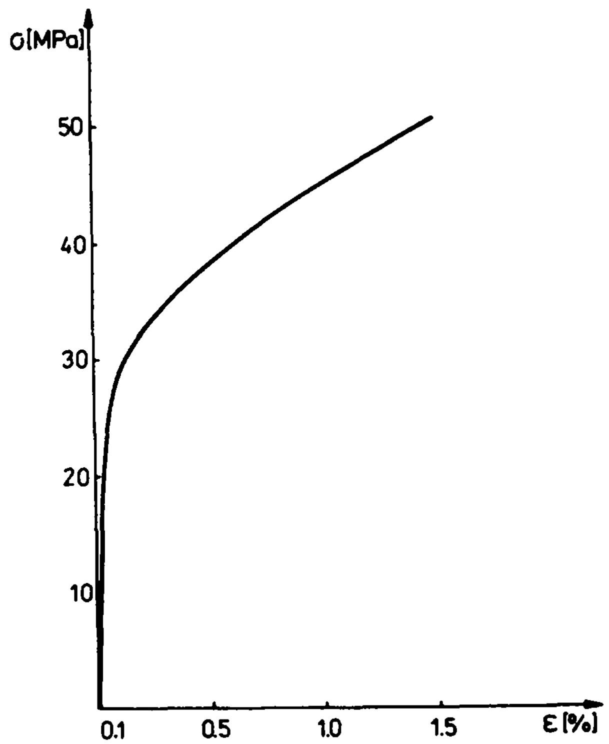

Fig. 3. Uniaxial stress–strain curve for copper tested at 300°C at constant strain rate $\dot{\epsilon}_x = 10^{-4}\,\mathrm{sec}^{-1}$.

procedure did not allow for precise measurement of such strains during reversals of shear stress, this effect is not included in the experimental curves. The time independent strains are presented only for initial loading (step 1) and the calculated creep curve is therefore shifted by instantaneous term according to the data shown in Fig. 3.

The material parameters for theoretical calculation of the creep loading and unloading processes were assumed as follows: $A = 20$ (eqn 26), $\beta = 0.02$, $\gamma = 0.0145$ (eqn 27), $B = 7$, $K = 1.5$ (eqn 34) when calculating stresses in [MPa].

The initial value of $\alpha_m = 0$ was changed to $\alpha_m = \alpha_f^{(0)} = 9.22$[MPa] during the initial loading process (eqn 26) and subsequently value $\alpha_f^{(0)}$ was changed due to cyclic process (eqn 27), so that $\alpha_f^{(1)} = 10.54$[MPa] at the end of step 5. It corresponds to $\alpha_f^{(1)} = 0.402\sigma_e$, and during the subsequent loading, step 6, there is $\alpha_f^{(2)} = 0.402\sigma_e = 12.21$[MPa]. Following τ_{xy} cyclic changes, steps 7 and 8, $\alpha_f^{(2)}$ increase to $\alpha_f^{(2)} = 13.58$[MPa] at the end of step 8. It is seen, that experimental creep curves are fairly well predicted by the present model. The predicted and measured creep rates at the steady state for subsequent steps are presented in Table 1. The highest discrepancy between predicted and measured rates occurs for the step 8. This may be due to intervening creep damage effect which was neglected in our model.

Assume the Robinson's damage accumulation rule

$$D = \sum_{i=1}^{n} \left(\frac{t_i}{t_{r_i}}\right) = \sum Di \tag{46}$$

where D denotes the total damage, t_i is the period of maintaining stress σ_i, t_{r_i} is the rupture life corresponding to σ_i. Applying this rule, it can be deduced that the step 8 of creep begins at the time equal to $0.63t_R$ and in view of the analysis of copper damage under biaxial stress state[20], it is seen that the tertiary portion of the creep curve can be expected at this step.

Figure 5 shows the evolution of the back stress α during the consecutive creep steps. Initially, during the stage 1, the α-path coincides with the line 0–1. When the shear stress is reversed, the α-path follows the line A–B, Fig. 5(d). This rule is corroborated by the

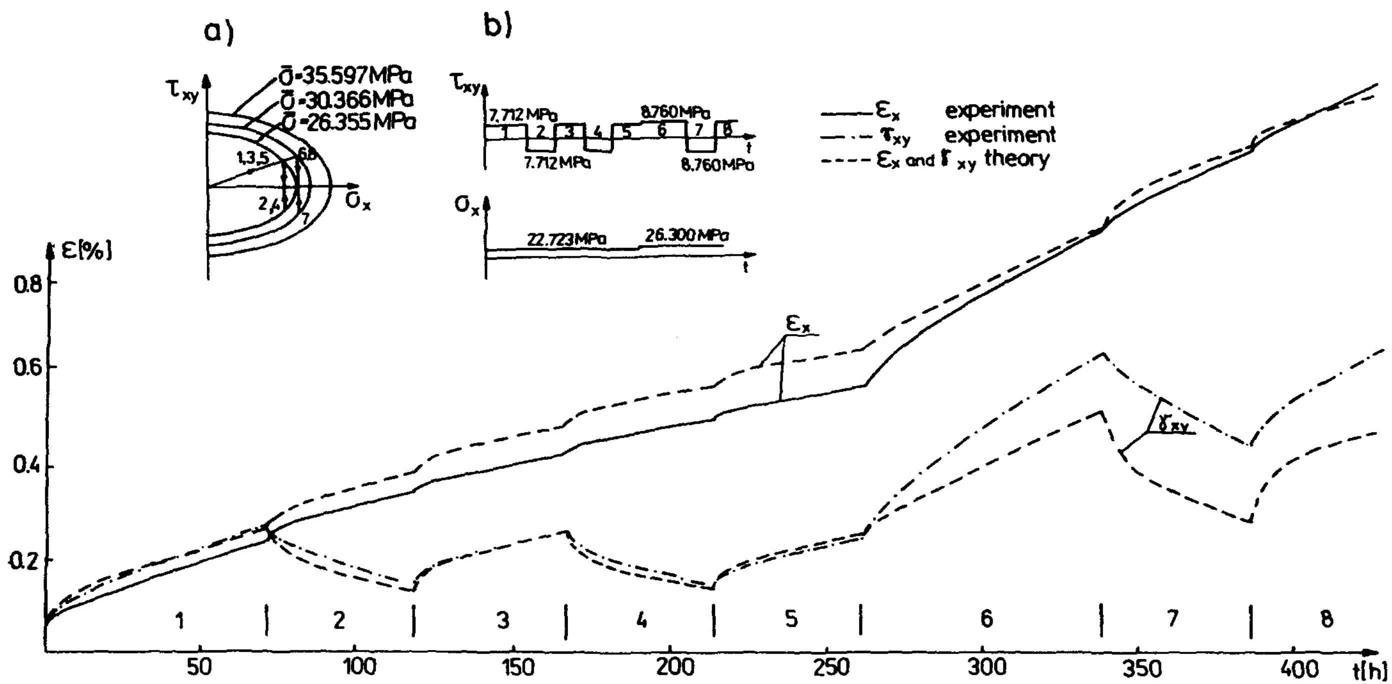

Fig. 4. Experimental and predicted creep curves of copper for cyclic torsion and constant axial stress. Loading Programme 1 is shown in insets (a) and (b).

Table 1. Steady state creep rates for particular loading steps

Period	Time h	Stress state MPa		Experiment $\dot{\varepsilon}_x \cdot 10^2$ [%/h]	Experiment $\dot{\gamma}_{xy} \cdot 10^2$ [%/h]	Theory $(\dot{\varepsilon}_x = \dot{\gamma}_{xy}) 10^2$ [%/h]
1	72	$\sigma_x = 22.723$ $\tau_{xy} = 7.712$	$\sigma_1 = 24.99$ $\bar{\sigma} = 26.355$	0.21	0.24	0.21
2	47	$\sigma_x = 22.723$ $\tau_{xy} = -7.712$		0.16	0.20	0.17
3	47	$\sigma_x = 22.723$ $\tau_{xy} = 7.712$		0.14	0.17	0.14
4	48	$\sigma_x = 22.723$ $\tau_{xy} = -7.712$		0.12	0.16	0.12
5	48	$\sigma_x = 22.723$ $\tau_{xy} = 7.712$		0.11	0.15	0.11
6	77	$\sigma_x = 26.300$ $\tau_{xy} = 8.760$	$\sigma_1 = 28.933$ $\bar{\sigma} = 30.366$	0.38	0.43	0.32
7	48	$\sigma_x = 26.300$ $\tau_{xy} = -8.760$		0.29	0.33	0.23
8	48	$\sigma_x = 26.300$ $\tau_{xy} = 8.760$		0.31	0.39	0.18

calculated α-path from the creep rule (34) by using measured creep rates, Fig. 5(e). In fact, the predicted α-path first moves from A in almost vertical direction and bends towards a radial line 0–2 in the vicinity of B. Figure 5(f) shows the evolution of α during the stage 3 of subsequent loading.

(ii) *Programme 2. Effect of overstress*

During this programme, the material was first subjected for the period of 19 hr to biaxial creep under higher stress state $\sigma_x = 30.711$[MPa], $\tau_{xy} = 10.393$[MPa], $\sigma_e = 35.597$[MPa] which resulted in creep strains much higher than those occurring at the end of the first step in Programme 1. Next, Programme 1 was executed. The following stages can therefore be distinguished:

—stage 1: Initial loading, step 1, $\sigma_x = 30.711$[MPa], $\tau_{xy} = 10.393$[MPa], $\sigma_e = 35.597$[MPa]
—stage 2: Unloading to $\sigma_e = 26.355$[MPa], step 2,
—stage 3: Cycling loading in torsion, steps 3–4, $\sigma_x = 22.723$[MPa], $\tau_{xy} = \pm 7.712$[MPa],
—stage 4: Subsequent loading, step 5, $\sigma_e = 30.366$[MPa],
—stage 5: Cycling loading in torsion, steps 6–7, $\sigma_x = 26.300$[MPa], $\tau_{xy} = \pm 8.760$[MPa].

During the last four hours of the first stage (initial loading) the strain rate of $\dot{\varepsilon}_x = 0.14[\%/h]$ was measured. It corresponds to the stress state $\sigma_x = 29.484$[MPa],

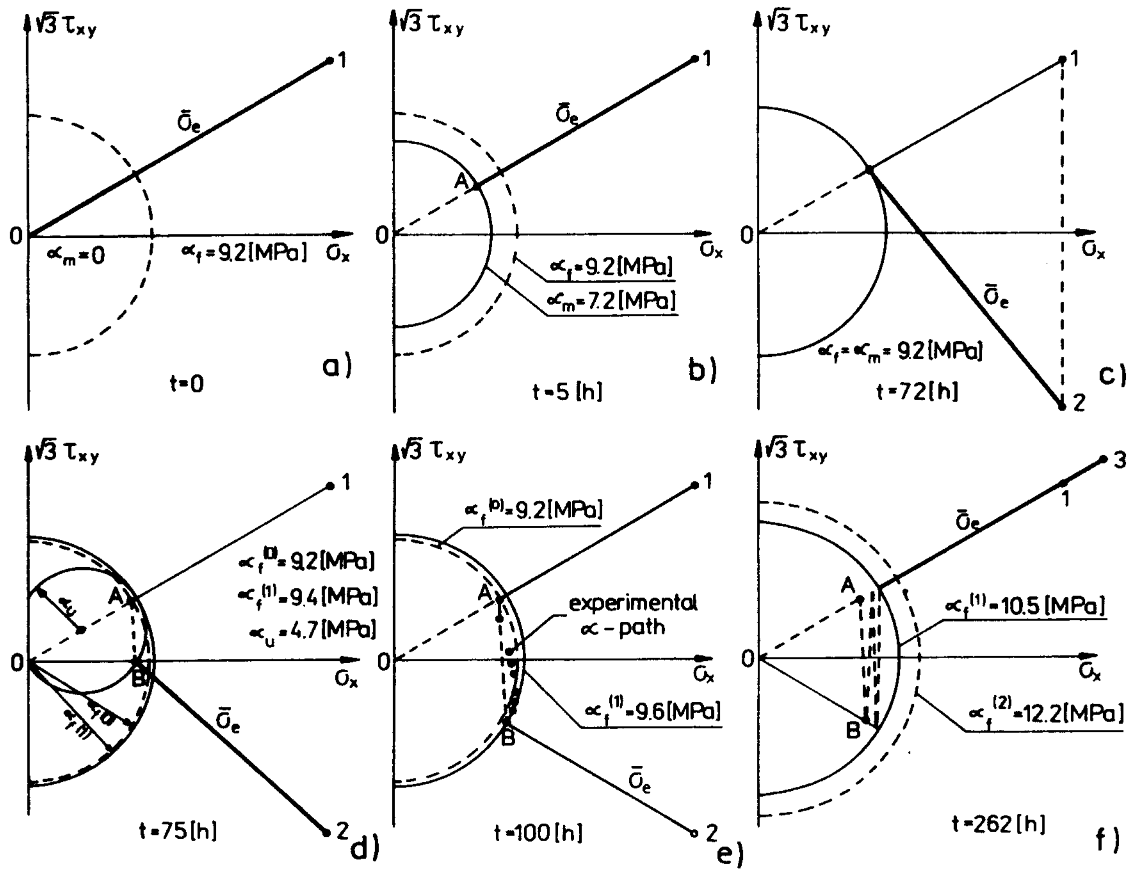

Fig. 5. Evolution of the back stress α for consecutive steps (Programme 1).

$\tau_{xy} = 9.973$[MPa], $\sigma_e = 34.17$[MPa] which is about 4% less than the applied stress state. Introducing the proper correction of the stress state the calculations, using the same material parameters as in Programme 1, were performed. Figure 6 shows experimental and predicted creep curves.

At the end of stage 1 there is $\alpha_m = \alpha_e = \alpha_f = 0.35\sigma_e = 11.96$[MPa] and when the specimen is unloaded to $\sigma_e = 26.355$[MPa] (after correction $\sigma_e = 25.3$[MPa]), step 2, the predicted value of $\alpha_f = 0.35$, $\sigma_e = 8.856$[MPa] is lower than $\alpha_f = \alpha_m$ reached during the first stage. Therefore $\dot{\alpha}_x^{(f)} = 0$, $\dot{\alpha}_f = 0$ according to (29) and only the evolution of α corresponding to the first term of (21) occurs. The evolution of α is shown in Fig. 7 and for the consecutive creep steps Table 2 provides the steady state creep rates for particular steps. It is seen that now creep rates are several times smaller than the respective rates for the same steps of Programme 1. This is due to initial overstress period during which a high value of $\alpha_m = \alpha_f = 11.96$[MPa] is attained and no further hardening nor relaxation occurs during subsequent cyclic loading.

(iii) *Programme* 3. *Effect of overstress, second programme*

This programme is similar to Programme 2. The material was first subjected for the period of 68 h to biaxial creep under stress state $\sigma_x = 26.3$[MPa], $\tau_{xy} = 8.76$[MPa] followed by unloading to $\sigma_x = 22.723$[MPa], $\tau_{xy} = 7.712$[MPa] and cycling loading in torsion, Fig. 8. The following stages of experiment can therefore be distinguished:

—stage 1: initial loading, step 1, $\sigma_e = 30.366$[MPa]
—stage 2: unloading to $\sigma_e = 26.355$[MPa], step 2
—stage 3: cycling loading in torsion, steps 3–6 ($\sigma_x = 22.723$, $\tau_{xy} = \pm 7.712$)
—stage 4: loading to initial stress state, $\sigma_e = 30.366$[MPa], step 7.

The strain rate $\dot{\epsilon}_x = 4 \times 10^{-3}$[%/$h$] for the steady state creep in stage 1 was measured. It corresponds to the stress state $\sigma_x = 24.985$[MPa], $\tau_{xy} = 8.32$[MPa], $\sigma_e = 28.844$[MPa] which is about 5% less than applied. As before, such stress state correction is taken in theoretical approach. Experimental results and predicted creep curves are shown in Fig. 8. During the initial loading, stage 1, α_f reaches the value $\alpha_m = \alpha_f = 10.1$[MPa] and when the specimen is unloaded to $\sigma_e = 26.355$[MPa] (corrected value $\sigma_e = 25.04$[MPa]), step 2, the predicted value of $\alpha_f = 8.864$[MPa] is lower than $\alpha_f = \alpha_m$ reached during the first stage. Therefore it is set $\dot{\alpha}^{(f)} = 0$, $\dot{\alpha}_f = 0$ and only the evolution of α corresponding to the first term of (22) occurs. Table 3 provides the steady state creep rates for particular steps. (For the steps 3–6, only the values of $\dot{\epsilon}_x$ are presented. It was found that the axial curve $\epsilon_x(t)$ reaches the steady state, after torsion change, earlier than the shear creep curve $\gamma_{xy}(t)$. During such short cycle period (48 h) the steady state was clearly seen for $\dot{\epsilon}_x$.) Creep rates at the stage 3 are five times smaller than the respective rates for the same step (1) of Programme 1. As before, this effect is due to the initial overstress and the prior creep hardening of the material.

4. CONCLUDING REMARKS

In the present model, the concept of kinematic hardening is used and the maximal prestress norm α_m provides the measure for active and unloading creep processes. Whereas the creep rule remains the same for two classes of processes, the evolution rules for α are different. The hardening and recovery phenomena are incorporated into the evolution rules and the interaction between monotonic and cyclic hardening can be simulated by using the effective and the accumulated scalar parameters α_m and α_a. The steady creep process is thus dependent on the loading history, in particular, on the cyclic creep process proceding the subsequent monotonic loading.

The experimental results and the model predictions are in fairly good agreement. The fundamental idea of this model, namely the memory of maximal prestress, provides sound description of creep effects for complex loading history. This is clearly seen when comparing experimental and theoretical steady creep strain rates for different loading programmes and steps shown in Tables 1–3. The effect of memory of maximal prestress

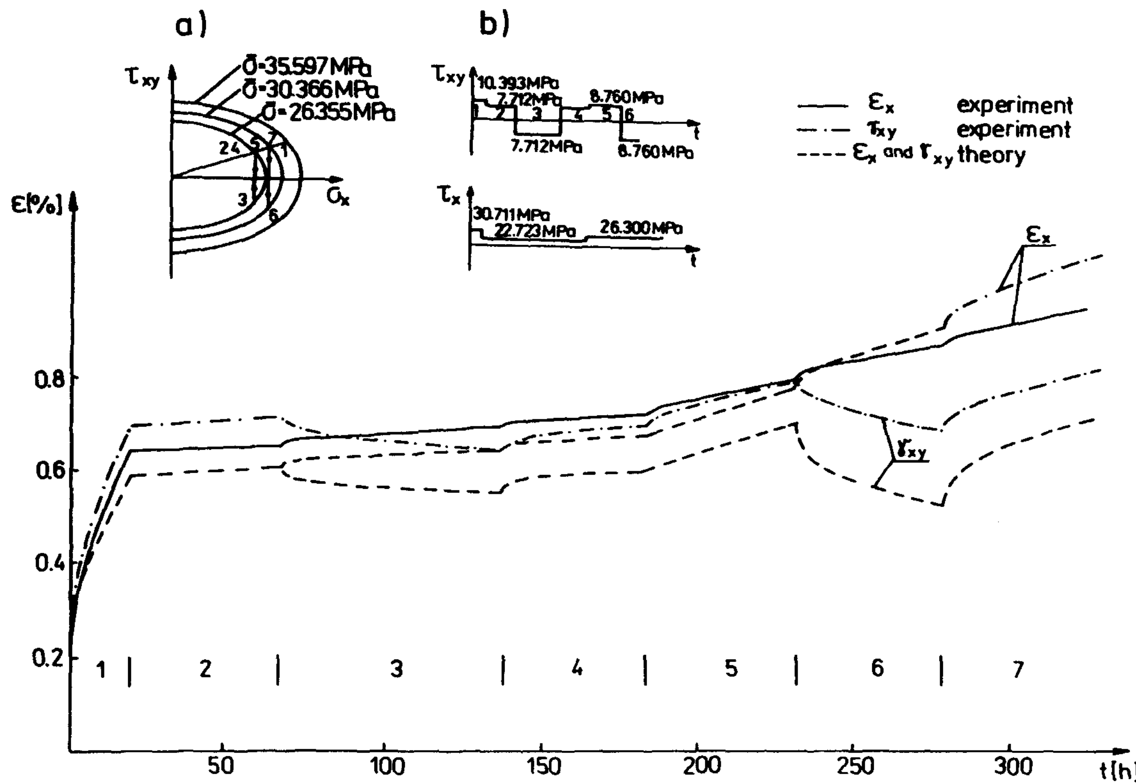

Fig. 6. Experimental and predicted creep curves for copper Programme 2 (shown in insets (a) and (b)).

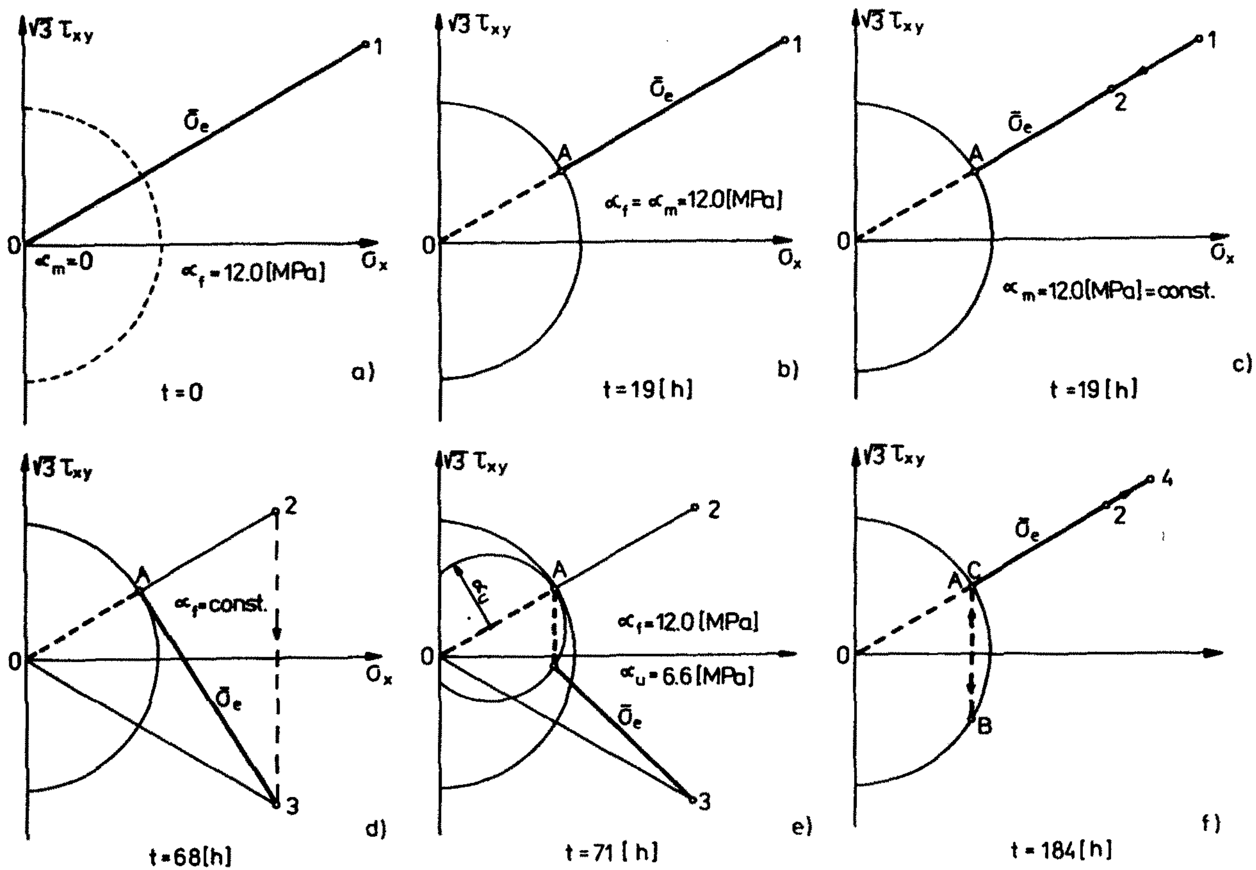

Fig. 7. Evolution of α for consecutive loading steps (Programme 2).

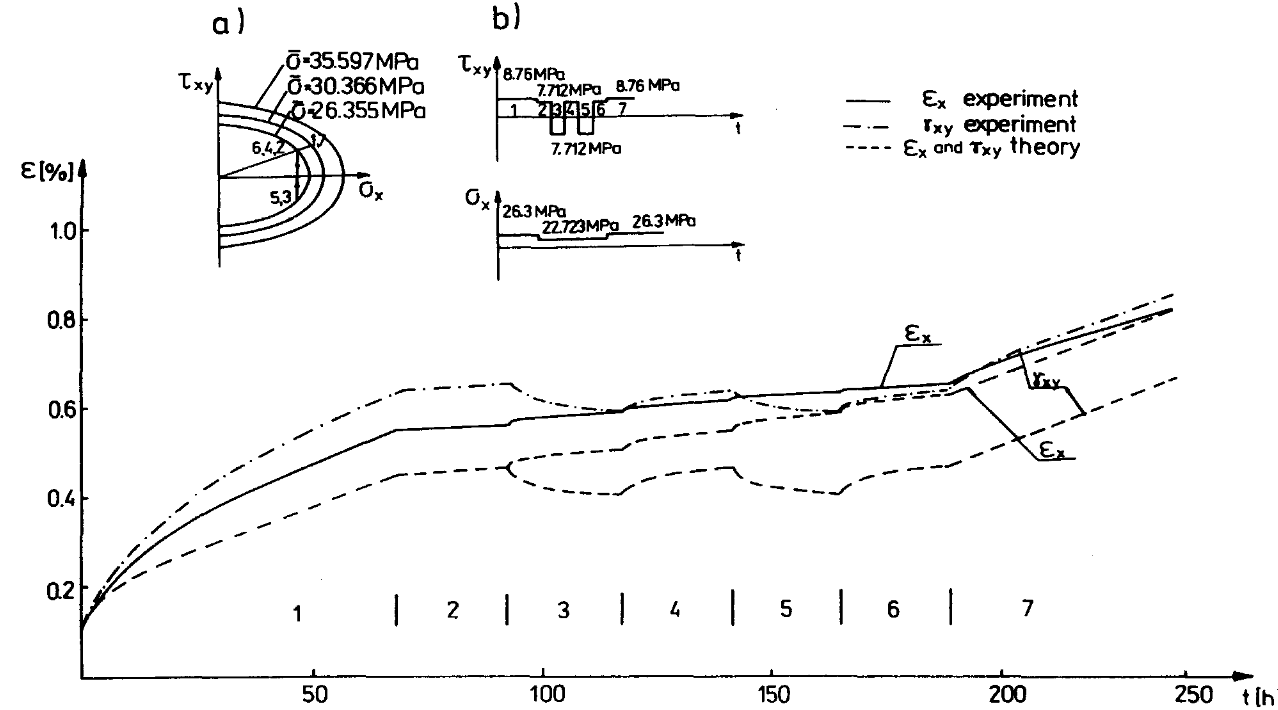

Fig. 8. Experimental and predicted creep curves of copper for Programme 3 (shown in insets (a) and (b)).

Table 2. Steady state creep rates for successive loading steps of Programme 2

Period	Time [h]	Stress state [MPa]	Experiment $\dot{\varepsilon}_x \cdot 10^2$ [%/h]	Experiment $\dot{\gamma}_{xy} \cdot 10^2$ [%/h]	Theory $(\dot{\varepsilon}_x = \dot{\gamma}_{xy}) 10^2$ [%/h]
1	19	σ_x=30.711 σ_1=33.778 τ_{xy}=10.393 $\bar{\sigma}$=35.597			
2	49	σ_x=22.723 σ_1=24.990 τ_{xy}= 7.712 $\bar{\sigma}$=26.355	0.040	0.048	0.033
3	70	σ_x=22.723 τ_{xy}=-7.712	0.043	0.058	0.033
4	46	σ_x=22.723 τ_{xy}= 7.712	0.042	0.061	0.033
5	47	σ_x=26.300 σ_1=28.933 τ_{xy}= 8.760 $\bar{\sigma}$=30.366	0.143	0.162	0.22
6	47	σ_x=26.300 τ_{xy}=-8.760	0.113	0.150	0.22
7	47	σ_x=26.300 τ_{xy}= 8.760	0.146	0.185	0.22

Table 3. Steady state creep rates for particular loading steps.

Period	Time [h]	Stress state [MPa]	Experiment $\dot{\varepsilon}_x \cdot 10^2$ [%/h]	Experiment $\dot{\gamma}_{xy} \cdot 10^2$ [%/h]	Theory $(\dot{\varepsilon}_x = \dot{\gamma}_{xy}) 10^2$ [%/h]
1	68	σ_x= 26.3 σ_1= 28.933 τ_{xy}= 8.76 $\bar{\sigma}$ = 30.366	0.40	0.46	0.40
2	24	σ_x= 22.723 σ_1= 24.99 τ_{xy}= 7.712 $\bar{\sigma}$= 26.355	0.051	0.058	0.078
3	25	σ_x= 22.723 τ_{xy}= -7.712	0.06		0.078
4	24	σ_x= 22.723 τ_{xy}= 7.712	0.058		0.078
5	24	σ_x= 22.723 τ_{xy}= -7.712	0.057		0.078
6	24	σ_x= 22.723 τ_{xy}= 7.712	0.055		0.078
7	48	σ_x= 26.3 σ_1 = 28.933 τ_{xy}= 8.76 $\bar{\sigma}$ = 30.366	0.35	0.41	0.40

can be found also in experimental data reported in [11] for polycrystalline copper at 413°C under uniaxial stress state. Using the approach of this work, good correlations can be found between experimental and theoretical results.

However, the description of primary creep during initial loading could not be described sufficiently well (Programmes 1–3, step 1). This is mainly due to simple relations describing this creep process (eqn 26). It is believed that this description can be improved provided more experimental results for transient creep under multiaxial stress state become available.

Similarly the description of primary creep during cyclic torsion is not fully satisfactory, especially for higher stress levels (Fig. 4, steps 7, 8; Fig. 6, steps 6, 7).

However, it is believed that the main features of creep process under complex loading histories are simulated with sufficient accuracy and further refinements together with new experimental programmes will be discussed in separate papers.

Acknowledgement—The experimental results discussed in this paper were obtained during the stay of Dr. W. Trąmpczyński at Leicester University, England, where he conducted the creep tests. The authors wish to express their gratitude to Profs. A. R. S. Ponter and R. Hayhurst for fruitful discussions on various aspects of creep of metals and for allowing the use of the laboratory facilities of Leicester University.

REFERENCES

1. Z. Mróz, On generalized kinematic hardening rule with memory of maximal prestress. *J. Mech. Appl.* **5**, 241–260 (1981).
2. D Kujawski and Z. Mróz, A viscoplastic material model and its application to cyclic loading. *Acta Mech.* **36**, 213–230 (1980).
3. F. A. Leckie and A. R. S. Ponter, On the state variable description of creeping materials. *Ing. Archiv.* **43**, 158–167 (1974).
4. N. N. Malinin and G. M. Khadjinsky, Theory of creep with anisotropic hardening. *Int. J. Mech. Sci.* **14**, 235–246 (1972).
5. E. W. Hart, Constitutive relations for non-elastic deformation of metals. *ASME J. Engng. Mat. Techn.* **98**, 193–202 (1976).
6. A. Miller, An inelastic constitutive model for monotonic, cyclic and creep deformation—I. Equation development and analytical procedures—II. Application to type 304 Stainless Steel. *ASME J. Engng. Met. Techn.* **98**, 97–105, 106–113 (1976).
7. B. Larsson and B. Storakes, A state variable interpretation of some rate-dependent inelastic properties of steel. *ASME J. Engng Mat. Techn.* **100**, 395–401 (1978).
8. J. L. Chaboche, Viscoplastic constitutive equations for the description of cyclic and anisotropic behaviour of metals. *Bull. Acad. Pol. Sci. Ser. Sci. Techn.* **25**, 33–39 (1977).
9. S. R. Bodner and A. Merzer, Viscoplastic constitutive equations for copper with strain rate history and temperature effects. *ASME J. Engng. Met. Techn.* **100**, 388–394 (1978).
10. E. P. Cernocky and E. Krempl, A theory of thermoviscoplasticity based on infinitesimal total strain. *Int. J. Solids Structures* **16**, 723–741 (1980).
11. J. D. Parker and B. Wilshire, Friction stress measurements during high temperature creep of polycrystalline copper. *Metal Sci.* 453–459 (Oct. 1978).
12. E. Krempl, On the interaction of rate and history dependence in structural metals. *Acta Mech.* **22**, 53–90 (1975).
13. J. L. Chaboche, K. Dang Van and G. Cordier, Modelization of the strain memory effect on the cyclic hardening of 316 Stainless Steel. *Trans. 5th Int. Conf. Struct. Mech. Reactor Techn.* (Edited by Jaeger T. A. and Boley B. A.). North-Holland, Amsterdam (1979).
14. S. Murakami and N. Ohno, A constitutive equation of creep based on the concept of a creep-hardening surface. *Int. Solids Structures* **18**, 567–609 (1982).
15. W. Trąmpczyński, C. Morrison and W. Topliss, A tension–torsion creep rupture testing machine. *J. Strain Anal.* **15**, 151–157 (1980).
16. J. F. Besseling, A theory of elastic plastic and creep deformation of an initially isotropic material showing anisotropic strain hardening, creep, recovery and secondary creep. *J. Appl. Mech.* **25**, 529–536 (1953).
17. P. Meijers, G. T. M. Janssen and J. Booij, Numerical elasticity and creep analysis based on the fraction model and experimental verification for AISI 304. *Trans. 3rd Int. Conf. Struct. Mech. React. Techn.* North Holland, London (1975).
18. Z. Mróz, On the description of anisotropic workhardening. *J. Mech. Phys. Solids* **15**, 163–175 (1967).
19. Y. Ohashi, N. Ohno and M. Kawai, Evaluation of creep constitutive equations for type 304 stainless steel under repeated multiaxial loading. *J. Engng. Mat. Techn.* **104**, 159–164 (1982).
20. W. Trąmpczyński, D. Hayhurst and F. Leckie, Creep rupture of copper and aluminium under non-proportional loading. *J. Mech. Phys. Solids* **29**, 353–374 (1981).